Direct Semiconductor Wafer Bonding in Noncleanroom Environment: Understanding the Environmental Influences on Bonding

AUTHOR NAMES

Ryoichi Inoue, Nagito Takehara, Takenori Naito, and Katsuaki Tanabe*

AUTHOR ADDRESS

Department of Chemical Engineering, Kyoto University, Nishikyo, Kyoto 615–8510, Japan

AUTHOR INFORMATION

Corresponding Author

*Email: tanabe@cheme.kyoto-u.ac.jp

KEYWORDS

Semiconductor, Wafer bonding, Surface, Interface, Electronics, Photonics, Device

ABSTRACT

We investigated semiconductor direct wafer bonding in a regular, noncleanroom environment to understand environmental influences on bonding characteristics. The correlations among surface treatments, particle densities, bonding strengths, and interfacial conductivities were systematically investigated. Based on our investigation and condition optimization, we realized direct semiconductor bonding in the regular atmosphere with high interfacial mechanical stabilities and electrical conductivities, sufficient for device applications. Furthermore, we demonstrated fabrication and operation of solar cells using the developed bonding technique, with current paths across the bonded interfaces. These results and related technical insights may be useful for a low-cost, simpler manufacture of high-performance electrical and optical devices.

MAIN TEXT

INTRODUCTION

Semiconductor wafer bonding is a versatile fabrication method used in various applications in electronics and photonics.[1–7] However, as particulates reduce the interfacial stability and conductivity in wafer bonding, the wafer bonding process is commonly carried out in cleanrooms (particle densities: ~1,000 m^{-3}), which leads to high operation costs. While many other processes related to electrical and optical devices are performed in the cleanrooms, some categories of large-area, relatively insensitive devices, such as solar cells, could be entirely fabricated in the normal atmosphere. In this study, we aim to realize direct semiconductor–to–semiconductor bonding without mediating agent in a noncleanroom, regular environment through an analysis of environmental effects on the semiconductor bonding represented by surface particulates, which can pave the way for low-cost mass productions of high-performance devices.

EXPERIMENTAL METHODS

In this study, we carried out all of the experimental processes in a noncleanroom regular environment with a particle density of approximately 5×10^6 m^{-3}, measured with a regular particle counter for particle sizes larger than 0.5 μm. We focused on the direct semiconductor–to–semiconductor wafer bonding without mediating agent, as the direct bonding is mostly influenced by environmental conditions represented by airborne particles, rather than on other bonding approaches such as those mediated by soft adhesive agents. The direct semiconductor wafer bonding is widely used in various optoelectronic devices, such as multijunction solar

cells,[8–10] owing to its simplicity and high interfacial optical transparency.

We used single-side-polished epi-ready *p*-type Si <100> wafers doped with boron (doping concentration of ~ 1×10^{19} cm^{-3}). Si wafers were diced into ~1 cm^2 pieces and were subjected to various wet chemical treatments, as discussed below. The polished sides of two Si piece surfaces were then contacted each other; their Si (011) edges were aligned. The two die pieces were then bonded by annealing at 300 ºC in ambient air for 3 h under a uniaxial pressure of 0.1 MPaG. We carried out the bondings at a fixed uniaxial pressure of 0.1 MPaG at 300 ºC for 3 h. We believe that these conditions are standard conditions for direct semiconductor bonding providing a good mechanical interfacial stability while avoiding the thermal expansion mismatch issue in heterogeneous bonding.[11–13] This enables a simple analysis of the results and comparison among various pre-bonding surface treatment conditions, which is the main objective of this study.

Before the bonding, we counted the particles on the Si wafer surface to be bonded using a regular optical microscope, to determine the areal density of particles observable with optical microscopy. After the bonding, the bonding interfacial strengths (normal stress) of the prepared samples were measured. The particle areal density on the Si wafer surface before the bonding process was measured through optical microscopy and scanning electron microscopy (SEM). For electrical measurements, metal electrodes comprising an Au–Ge–Ni alloy (80:10:10 wt:wt:wt) and pure Au with thicknesses of 30 and 150 nm, respectively, were sequentially deposited by thermal evaporation as ohmic electrodes on both outer Si surfaces of the bonded samples.

RESULTS AND DISCUSSION

I. Particle analysis

Figure 1 shows a set of SEM images of typical particles on the Si wafer surface and their Feret diameters. The Feret diameters of the particles were determined by using a graphic analysis software (*ImageJ*, National Institutes of Health) from the SEM images. The third (Feret diameter: 2.7 μm) and other images show Si particles generated in the dicing process and airborne dust particles adsorbed on the Si wafer, respectively. Figure 2 shows an energy-dispersive X-ray (EDX) spectrum of typical particles adsorbed on the wafer surface from the atmosphere. We detected major amounts of metal elements in the EDX spectrum. However, it should be noted that the large Si peak is partly attributed to the Si wafer. The detected Cu and Zn peaks may be partially attributed to our SEM stage consisting of a brass material. The airborne particles are thus considered to be mostly metals and/or metal oxides, according to our elemental analysis.[14–18] As metal particles and metal oxide particles are mechanically quite solid and are not flattened at the bonding interface even in highly pressed bonding processes, such particles would be a substantial obstacle in the formation of bonds. Therefore, it is very important to minimize the number of particles on the bonding surface to provide better interfacial properties.

Figure 3 shows a typical distribution of Feret diameters of the particles on the Si wafer surface, which were counted using SEM and optical microscopy for smaller and larger regions, respectively. For simplicity, for each condition, we represent the areal particle density on the wafer surface considering the particles with Feret diameters larger than 1 μm, which are countable by optical microscopy. Even during the pre-bonding processes for the semiconductor wafers, the surface particle density increases, particularly in regular noncleanroom environments. Figure 4 shows a typical time evolution of the areal particle density on the Si wafer surface

measured in our experimental room. For such a low-coverage-fraction regime, the areal particle density increases approximately proportionally to the time.[19] In the regular noncleanroom experimental environment, the particle density on the semiconductor wafer increases at a rate of approximately 70 cm^{-2}/h (i.e., ~1.2 cm^{-2}/min, ~1700 cm^{-2}/day) when the wafer surface is exposed to the air. Therefore, the fractional increase in the surface particle density is trivial for the typical pre-bonding process duration on the order of ~10 min. However, the long-term storage of semiconductor wafers may be problematic considering these particle-increment data. The particle increment can be completely suppressed simply by storing the wafers in sealed cases, which yielded an increase of only tens of particles in square centimeter per day.

II. Blowing process

Air and nitrogen blowers are often used to remove dust particles from semiconductor surfaces and to remove liquids from the surface after wet chemical treatments. We measured the change in particle density on the wafer surface under air blowing using a regular blower gun sourced by a house compressed-air supply gas line. Figure 5 shows the relationship between the surface particle density and time of blowing onto the wafer surface. According to the experimental data, the particle density significantly increases with the blowing time, which could be attributed to two factors. First, particles might come out of the blower gun and adsorb onto the wafer surface. Second, particles existing in the atmosphere of the experimental room might be pushed by the blower to adsorb onto the wafer surface. As we observed a similar particle density increase when we tested a reproduction of the blowing effect without using the blower gun by fanning the wafer with a paper fan with a similar air velocity to that of the blower gun, the latter is the most likely origin of the particle density increase. This shows that the regular blowing process commonly carried out in cleanrooms causes a significant increase in the number of surface particles by

pushing the environmental particulates onto the wafer surface particularly in noncleanroom environments. Therefore, we employed procedures to minimize the blower use, as described below. It is worth noting that in a regular noncleanroom environment, the surface particle increase by the blowing process is significantly larger than that by the natural spontaneous adsorption in the atmosphere, as shown in Fig. 4 for the typical duration of the pre-bonding treatment processes. Further, regarding the blower's pressure, we need to determine whether a short-time blow (requiring a higher pressure) to suppress the surface-particle increase and complete the blowing process, e.g., to remove water droplets from the wafer surface, is preferable over a soft gentle blow carried out over a longer time. The results show that a relatively gentle blow for a long time to complete the blowing process is preferable owing to the smaller increase in the total particle density, over a high-velocity blow for a shorter time, as shown in Fig. 6. Therefore, we set the air pressure of the blower gun at 0.05 MPa for the subsequent analyses.

III. Strategy against particle generation in the wafer dicing process

Further, we consider the wafer cutting process. When we dice a semiconductor wafer into smaller pieces, small fragment pieces are generally generated out of the wafer and then adsorbed as particulates and also surface scratches are created, which could affect the proper interface formation in the wafer bonding. The particles generated in the cutting procedure could be removed by blowing. However, we demonstrated that the blowing process leads to a significant increase in the number of surface particles, particularly in the regular noncleanroom ambient atmosphere; therefore, we employed an alternative surface coating technique.[8,12] In this approach, the Si wafers were spin-coated with a photoresist before the cutting process into the die pieces to be bonded, in order to protect the bonding surface from particles generated during

the cutting process. Immediately before the bonding, the photoresist on both dies was removed with acetone and the bonding surfaces were degreased, as illustrated in the flow diagram in Fig. 7. This surface-coating scheme provides an advantage that particulates and scratches are formed on the coating material but not on the semiconductor surface as the coating is present in the cutting process. The particles are then completely easily coremoved with the coating material by the chemical solvent, providing a clean pristine semiconductor surface. According to our experimental tests (Fig. 8), for the cases with and without the surface coating treatment in the cutting process, the surface-coating treatment in the dicing process used to minimize the particulate adsorption led to a more than twice smaller particle density and more than twice higher bonding strength. Therefore, we employed the surface coating scheme for the bonding experiments presented in the following sections.

IV. Interfacial mechanical strength

As we demonstrated the importance to minimize the blowing process to suppress the surface particle adsorption, we investigate alternative methods to dry the semiconductor surface after the chemical wet treatments. The first method is spin drying, which was used to remove water droplets from the semiconductor (Si in this study) surface through the centrifugal force using a regular spinner with a rotation velocity of 7000 rpm for 5 s. The second method is heat drying, where we heated the Si pieces on a regular hotplate at 100 ºC to evaporate and eliminate water from the Si surface, which takes about 10 s. The third method is hydrophobization of the Si surface by an HF solution. We dipped the Si pieces in HF aq. (10 vol%) for 1 min followed by a deionized-water rinsing prior to the bonding, so that water droplets could be eliminated even without any physical water removal with methods such as blowing, spinning, and heating. Additionally, we tested bonding without removal of water on the Si surfaces. Figure 9 shows the

surface particle density prior to the bonding and mechanical interfacial bonding strength for each drying process for the four alternative methods described above, along with the case with the conventional blow drying. For this comparison, we unified the process flow conditions. We did not use additional chemical treatments (presented below) but only deionized-water rinsing after the photoresist-coating removal by acetone, to compare the drying processes of water prior to the bonding. As shown in Fig. 9, all of the four alternative methods without using the blower provided significantly lower surface particle densities. Except for the HF hydrophobization scheme, a clear relationship between the particle density and bonding strength is observed. Therefore, we significantly enhanced the mechanical stability of the bonded interface by applying the alternative methods. It is worth noting that the bonding with the remaining surface water provided the highest bonding strength among those of the considering processes. This can be attributed to the formation of oxide bridges,[1,20] as depicted in Fig. 10, and/or to the higher promotion of bond formation owing to the interwater attractive dragging force from the surface tension induced by the vaporization of interfacial water in the bonding annealing.[21] The surface hydrophobization scheme provided a very low particle density but led to a relatively low bonding strength, presumably owing to the absence of the oxygen bridge and/or surface tension effects. However, as the interfacial electrical conductivity is also an important factor for many optoelectronic device applications, we consider such hydrophobic bonding below.

Further, we introduced an ultrasonication surface cleaning using a regular ultrasonication bath with a frequency of 37 kHz. It is expected that the ultrasonic cleaning could remove the surface particles by the cavitation effect. We tested surface treatments with deionized water and acetone with and without sonication for a bonding without removal of water on the Si surfaces. Figure 11 shows the obtained surface particle density after each surface cleaning treatment for 10 min prior

to the bonding and corresponding bonding strength. A significant reduction in the number of surface particulates is observed upon the ultrasonication cleaning treatment. Therefore, along with the obtained enhancement in bonding strength, the effectiveness of the sonication process is demonstrated. Further, we carried out a series of tests with varied time of ultrasonication. Figure 12 shows the obtained surface particle density after each sonication prior to the bonding and corresponding bonding strength. We have not yet established clear correlations among the sonication time, particle density, and bonding strength. Presumably, the obtained bonding strength is not affected by the variations in the process conditions; however, some random fluctuations are observed. We achieved a bonding interfacial mechanical strength as high as 1.2 MPa, which is comparable to the state-of-the-art reported data obtained in cleanrooms from leading research teams in the field,[22,23] and sufficient stability for device applications. As shown in the typical cross-sectional SEM image of the bonded Si/Si interface in Fig. 13, the wafers are firmly and uniformly contacted each other with a sufficient mechanical stability to endure the cleavage of the bonded-pair sample.

V. Interfacial electrical conductivity

For hydrophilic bonding, owing to the oxygen bridges such as Si–O–Si at the bonded interface, the bonding mechanical strength tends to increase for a certain range of conditions.[1,20] However, for many device applications, interfacial electrical conductivity, not only mechanical stability, is important. We investigate the electrical properties of the bonded interfaces through current–voltage measurements of the bonded-wafer-pair samples. Particularly, for the electric conductance across the bonded interface, we additionally investigate a pre-bonding contacting process in HF aq., in addition to the five drying methods described above. After the pre-bonding contacting in HF aq., no rinsing was carried out prior to the bonding because the little HF aq.

residue on the outer surfaces of the bonded-pair sample does not matter for the bonding interfacial characteristics and instantaneously dries out due to the hydrophobicity. Figure 14 shows the current–voltage characteristics across the bonded Si/Si interfaces obtained by the various surface treatments. Figure 15 shows the X-ray photoelectron spectroscopy (XPS) spectra of debonded Si surfaces immediately after the intentional debonding of the bonded samples obtained by different pretreatments. We referred Ref. 24 for the Si and SiO_2 peak energy regions in XPS analysis. Table 1 presents the ratios of the peak area of SiO_2 to that of Si in the XPS measurements (Fig. 15) of the bonded samples. They represent the amounts of SiO_2 on the Si surfaces to be bonded after the surface pretreatments. According to Fig. 14 and Table 1, a smaller surface SiO_2 content corresponds to a higher bonding interfacial electrical conductivity. A significant influence of the interfacial residual water, which may induce the formation of silicon oxide at the bonded interface, on the interfacial electrical properties was observed. Specifically, among the surface drying processes, the heating evaporation might better eliminate water than the physical blowing and spinning schemes. The chemical surface hydrophobization by HF provided a high interfacial electrical conductivity owing to the removal of the electrically insulating surface oxide, SiO_2. Additionally, we evaluated the interfacial electrical conductances for other doping concentrations in the Si wafers (in addition to the case of $\sim 1 \times 10^{19}$ cm^{-3}). Figure 16 shows the dependences of the current–voltage characteristics on the doping concentration, for the samples obtained by HF hydrophobization and heat drying.

Further, we additionally introduce the RCA SC-1 wet chemical cleaning,[25–27] for superior processes along with the heat drying and HF hydrophobization. The SC-1 cleaning removes surface particles by repeated formation and dissolution of silicon oxide through lifting-off of the particles from the surface. It also sets the wafer and particle zeta potentials negative to ease the

desorption of particles adsorbed electrostatically. Figure 17 shows the surface particle densities and interfacial electrical resistivities for the cases with an SC-1 cleaning (NH_3:H_2O_2:H_2O = 13:17:70 wt:wt:wt) for 10 min, ultrasonic cleaning in deionized water for 2 min, and without these treatments. Regarding the interfacial electrical resistivities, it should be noted that all of the current–voltage characteristics presented in this paper, such as those in Figs. 14 and 16, include all of the series resistances through the samples. Therefore, we independently determined the contact resistance of the metal electrode/semiconductor interface by the transmission line method, and then determined the nominal resistivity at the bonded interface by subtracting it from the slope of the current–voltage curve. As shown in Fig. 17, as for the ultrasonication treatment, the SC-1 cleaning significantly reduced the surface particle density and interfacial electrical resistivity, except for the case with the heat drying after the SC-1 treatment, which demonstrates the effectiveness of this cleaning scheme for a successful semiconductor wafer bonding particularly for the case of operation in regular noncleanroom environments. The high interfacial electrical resistance of the sample subjected to the heat drying after the SC-1 treatment can be attributed to oxide generation in the SC-1 dipping. Figure 18 shows the dependence of the current–voltage characteristic on the doping concentration in the Si wafers for the sample obtained by the SC-1 cleaning followed by pre-bonding contacting in HF aq. We obtained an ohmic bonded interface with an electrical resistivity as low as 0.025 Ω cm^2 when we employed the SC-1 surface cleaning before the hydrophobization (Fig. 17). Furthermore, an ohmic interface with a resistivity of 0.018 Ω cm^2 was obtained for the bonded sample subjected to the SC-1 cleaning followed by pre-bonding contacting in HF aq. (Fig. 18). The large effect of the combination of SC-1 cleaning and pre-bonding contacting in HF aq. can be attributed to the simultaneous suppression of surface particulates and oxide formation by the contact of the

surfaces to be bonded without exposure to the air after the oxide removal. The obtained high-electrical-conductivity semiconductor interfaces are suitable for use in most optoelectronic devices.

VI. Device fabrication and operation demonstration

Using the developed direct bonding technique, we fabricated Si solar cells bonded to Si wafers to demonstrate the applicability of our bonded semiconductor interface in optoelectronic devices. Si solar cells were prepared by thermal diffusion of phosphorus (10^{19}–10^{20} cm^{-3}) into one side of the surface region of a double-side-polished epi-ready *p*-type Si <100> wafers doped with boron (doping concentration of ~ 1×10^{16} cm^{-3}). After the phosphorus thermal diffusion, the boron doping concentration on the other surface was increased to the level of 10^{19}–10^{20} cm^{-3} by ion implantation, in order to provide a sufficient electrical conductance at the bonded interface. The *p*-type side of the Si solar cell wafer was bonded to a bare Si wafer (the same wafer used for the above bonding investigation) under the same process conditions as those in the bonding investigation, including the SC-1 cleaning and in-HF contacting, providing the highest conductivity according to the bonding investigation. A front grid contact on top of the Si cell and bottom contact on the back of the bare Si wafer were formed with the Au/Au–Ge–Ni metal material in the same manner as in the bonding investigation. It should be noted that, in this electrode configuration, the current passes through the bonded interface during the solar cell operation. Therefore, these solar cell fabrication and operation test are suitable to evaluate the validity of our bonding scheme for optoelectronic device applications. For comparison, we also prepared a pristine reference solar cell sample from the same Si solar cell wafer with the same top and bottom electrodes, which was not bonded with a bare Si wafer but was standing alone. Figure 19 depicts schematic cross-sectional structural diagrams of the bonded and reference Si

solar cells.

We fabricated six bonded Si solar cells and twelve reference cells. We fabricated more reference cells than bonded cells as we observed statistical variations in cell performance. The bonded cells were unexpectedly better than the reference cells, and thus we additionally prepared more reference cells. Figure 20 shows the light current–voltage characteristics of the best bonded and best reference cells under AM1.5 G, 1-sun (100 mW cm^{-2}) illumination. The performance of the bonded cell was slightly lower than that of the reference cell (e.g., the energy-conversion efficiencies η of the bonded and reference cells were 7.5% and 8.0%, respectively). However, as mentioned above, our fabricated cells exhibited statistical fluctuations in their performances. Table 2 presents the average solar cell performance parameters (open-circuit voltage V_{OC}, short-circuit current density J_{SC}, fill factor FF, and η) statistically averaged for each of the bonded and reference cells. As observed in this statistics, the performances of the bonded cells were comparable to those of the unbonded reference cells. For example, the average η values of the bonded and reference cells were 6.7% and 6.2%, respectively; the bonded cells were slightly better than the reference cells. Therefore, the bonding process and the bonded interface did not degrade the solar cell and its performance, and thus our bonding scheme is applicable for optoelectronic devices.

CONCLUSIONS

In this study, we investigated the semiconductor direct wafer bonding in a regular noncleanroom environment to understand the environmental influences on the bonding. We focused on the direct semiconductor–to–semiconductor wafer bonding without mediating agent,

as the direct bonding is influenced mostly by environmental conditions represented by airborne particles, rather than on other bonding schemes such as those mediated by soft adhesive agents. Based on the systematic investigation and condition optimization, we realized the direct semiconductor bonding in the regular atmosphere with sufficiently high interfacial mechanical strength and electrical conductivity for device applications. Furthermore, we demonstrated fabrication and operation of solar cells using the developed bonding technique with current paths across the bonded interfaces. The presented bonding scheme and related technical insights may be useful to manufacture high-performance semiconductor electronic and photonic devices at low costs.

AUTHOR INFORMATION

Corresponding Author

*Email: tanabe@cheme.kyoto-u.ac.jp

Group page: http://www.cheme.kyoto-u.ac.jp/5koza/index_e.htm

ORCID

Katsuaki Tanabe: 0000-0002-0179-4872

Notes

The authors declare no competing financial interest.

ACKNOWLEDGMENT

The authors would like to thank Noriaki Sano of Kyoto University for his support on the EDX spectroscopy measurements, and Yuan-Hsuan Jhang of the University of Tokyo for the discussion. This study was financially partly supported by the Kansai Research Foundation for Technology Promotion, Research Foundation for Electrotechnology of Chubu, and Japan Society for the Promotion of Science.

REFERENCES

(1) Tong, Q.; Goesele, U. M. Wafer bonding and layer splitting for microsystems. *Adv. Mater.* **1999**, *11*, 1409–1425.

(2) Noda, S.; Tomoda, K.; Yamamoto, N.; Chutinan, A. Full three-dimensional photonic bandgap crystals at near-infrared wavelengths. *Science* **2000**, *289*, 604–606.

(3) Celler, G.K.; Cristoloveanu, S. Frontiers of silicon-on-insulator. *J. Appl. Phys.* **2003**, *93*, 4955–4978.

(4) Van Campenhout, J.; Rojo-Romeo, P.; Regreny, P.; Seassal, C.; Van Thourhout, D.; Verstuyft, S.; Di Cioccio, L.; Fedeli, J. M.; Lagahe, C.; Baets, R. Electrically pumped InP-based microdisk lasers integrated with a nanophotonic silicon-on-insulator waveguide circuit. *Opt. Express* **2007**, *15*, 6744–6749.

(5) Palit, S.; Kirch, J.; Tsvid, G.; Mawst, L.; Kuech, T.; Jokerst, N. M. Low-threshold thin-film III–V lasers bonded to silicon with front and back side defined features. *Opt. Lett.* **2009**, *34*, 2802–2804.

(6) Madsen, M.; Takei, K.; Kapadia, R.; Fang, H.; Ko, H.; Takahashi, T.; Ford, A. C.; Lee, M. H.; Javey, A. Nanoscale semiconductor "X" on substrate "Y" – Processes, devices, and applications. *Adv. Mater.* **2011**, *23*, 3115–3127.

(7) Crosnier, G.; Sanchez, D.; Bouchoule, S.; Monnier, P.; Beaudoin, G.; Sagnes, I.; Raj, R.; Raineri, F. Hybrid indium phosphide-on-silicon nanolaser diode. *Nature Photon.* **2017**, *11*, 297–300.

(8) Tanabe, K.; Fontcuberta i Morral, A.; Atwater, H. A.; Aiken, D. J.; Wanlass, M. W. Direct-bonded GaAs/InGaAs tandem solar cell. *Appl. Phys. Lett.* **2006**, *89*, 102106.

(9) Dimroth, F.; Grave, M.; Beutel, P.; Fiedeler, U.; Karcher, C.; Tibbits, T. N. D.; Oliva, E.; Siefer, G.; Schachtner, M.; Wekkeli, A.; Bett, A. W.; Krause, R.; Piccin, M.; Blanc, N.; Drazek, C.; Guiot, E.; Ghyselen, B.; Salvetat, T.; Tauzin, A.; Signamarcheix, T.; Dobrich, A.; Hannappel, T.; Schwarzburg, K. Wafer bonded four-junction GaInP/GaAs//GaInAsP/GaInAs concentrator solar cells with 44.7% efficiency. *Prog. Photovolt.* **2014**, *22*, 227–282.

(10) Essig, S.; Allebé, C.; Remo, T.; Geisz, J. F.; Steiner, M. A.; Horowitz, K.; Barraud, L.; Ward, J. S.; Schnabel, M.; Descoeudres, A.; Young, D. L.; Woodhouse, M.; Despeisse, M.; Ballif, C.; Tamboli, A. Raising the one-sun conversion efficiency of III–V/Si solar cells to 32.8% for two junctions and 35.9% for three junctions. *Nature Ener.* **2017**, *2*, 17144.

(11) Fang, A. W.; Park, H.; Cohen, O.; Jones, R.; Paniccia, M. J.; Bowers, J. E. Electrically pumped hybrid AlGaInAs-silicon evanescent laser. *Opt. Express* **2006**, *14*, 9203–9210.

(12) Tanabe, K.; Watanabe, K.; Arakawa, Y. III-V/Si hybrid photonic devices by direct fusion bonding. *Sci. Rep.* **2012**, *2*, 349.

(13) Naito, T.; Tanabe, K. Fabrication of Si/graphene/Si double heterostructures by semiconductor wafer bonding towards future applications in optoelectronics. *Nanomater.* **2018**, *8*, 1048.

(14) Linton, R. W.; Loh, A.; Natusch, D. F. S.; Evans, Jr., C. A.; Williams, P. Surface predominance of trace elements in airborne particles. *Science* **1976**, *191*, 852–854.

(15) Fukino, H.; Miura, S.; Inoue, K.; Yamane, Y. Correlations among atmospheric elements, airborne particulate matter, benzene extracts, benzo(a)pyrene, NO, NO_2 and SO_2 concentrations in Japan. *Atmos. Environ.* **1984**, *18*, 983–988.

(16) Janssen, N. A. H.; van Mansom, D. F. M.; van der Jagt, K.; Harssema, H.; Hoek, G. Mass concentration and elemental composition of airborne particulate matter at street and background locations. *Atmos. Environ.* **1997**, *31*, 1185–1193.

(17) Sanchez Jimenez, A.; Heal, M. R.; Beverland, I. J. Correlations of particle number concentrations and metals with nitrogen oxides and other traffic-related air pollutants in Glasgow and London. *Atmos. Environ.* **2012**, *54*, 667–678.

(18) Fukushima, S.; Zhang, D. Comparison in size and elemental composition of dust particles deposited to the surface and suspended in the air on the southwest Japan coast. *Atmos. Environ.* **2015**, *118*, 157–163.

(19) Tanabe, K. Modeling of airborne dust accumulation on solar cells at the Martian surface. *Acta Astro.* **2008**, *62*, 683–685.

(20) Shimbo, M.; Furukawa, K.; Fukuda, K.; Tanzawa, K. Silicon-to-silicon direct bonding method. *J. Appl. Phys.* **1986**, *60*, 2987–2989.

(21) Liau, Z. L. Semiconductor wafer bonding via liquid capillarity. *Appl. Phys. Lett.* **2000**, *77*, 651–653.

(22) Takagi, H.; Maeda, R.; Chung, T. R.; Hosoda, N.; Suga, T. Effect of surface roughness on room-temperature wafer bonding by Ar beam surface activation. *Jpn. J. Appl. Phys.* **1998**, *37*, 4197–4203.

(23) Hayashi, Y.; Osabe, R.; Fukuda, K.; Atsumi, Y.; Kang, J. H.; Nishiyama, N.; Arai, S. Low threshold current density operation of a GaInAsP/Si hybrid laser prepared by low-temperature N_2 plasma activated bonding. *Jpn. J. Appl. Phys.* **2013**, *52*, 060202.

(24) Flitsch, R.; Raider, S. I. Electron mean escape depths from x-ray photoelectron spectra of thermally oxidized silicon dioxide films on silicon. *J. Vac. Sci. Technol.* **1975**, *12*, 305–308.

(25) Kern, W.; Puotinen, D. A. Cleaning solutions based on hydrogen peroxide for use in silicon semiconductor technology. *RCA Rev.* **1970**, *31*, 187–206.

(26) Kern, W. The evolution of silicon wafer cleaning technology. *J. Electrochem. Soc.* **1990**, *137*, 1887–1892.

(27) Itano, M.; Kern, F. W.; Miyashita, M.; Ohmi, T. Particle removal from silicon wafer surface in wet cleaning process. *IEEE Trans. Semicond. Manufacturing* **1993**, *6*, 258–267.

FIGURES

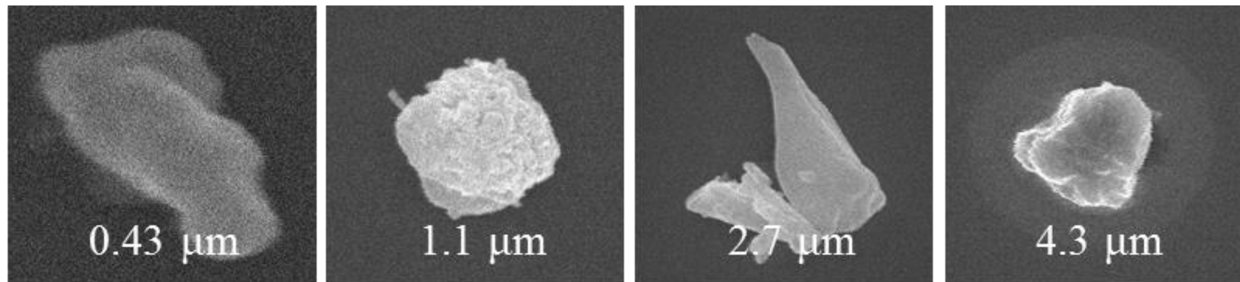

Figure 1. SEM images of typical particles adsorbed on the wafer surface from the atmosphere and their Feret diameters.

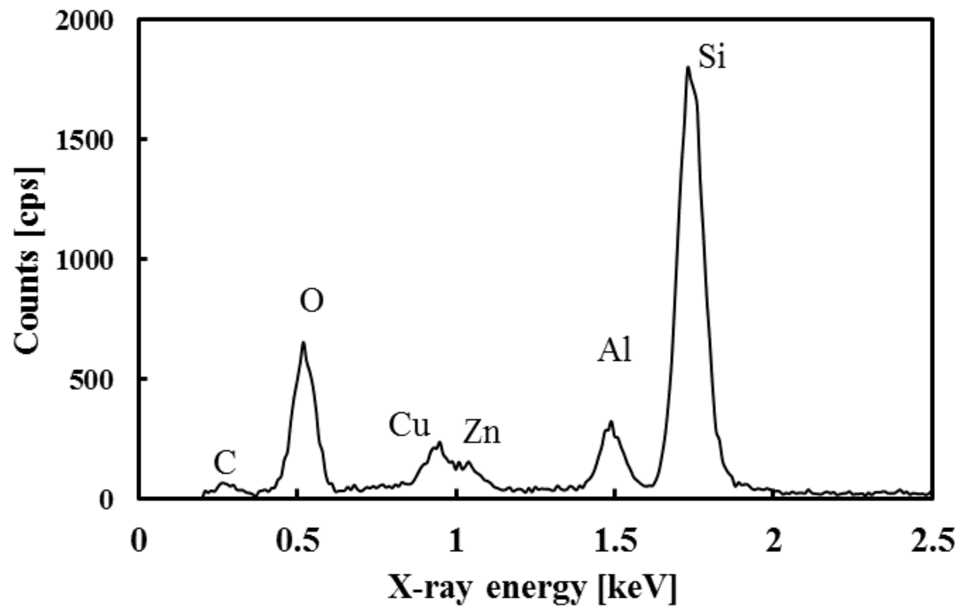

Figure 2. EDX spectrum of typical particles adsorbed on the wafer surface from the atmosphere.

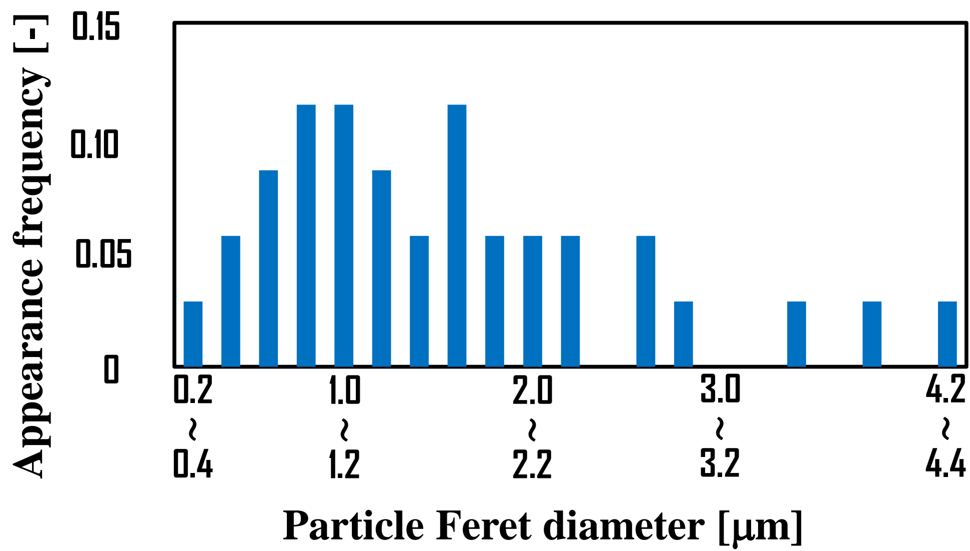

Figure 3. Typical distribution of Feret diameters of the particles on the Si wafer surface counted using SEM and optical microscopy for the smaller and larger regions, respectively.

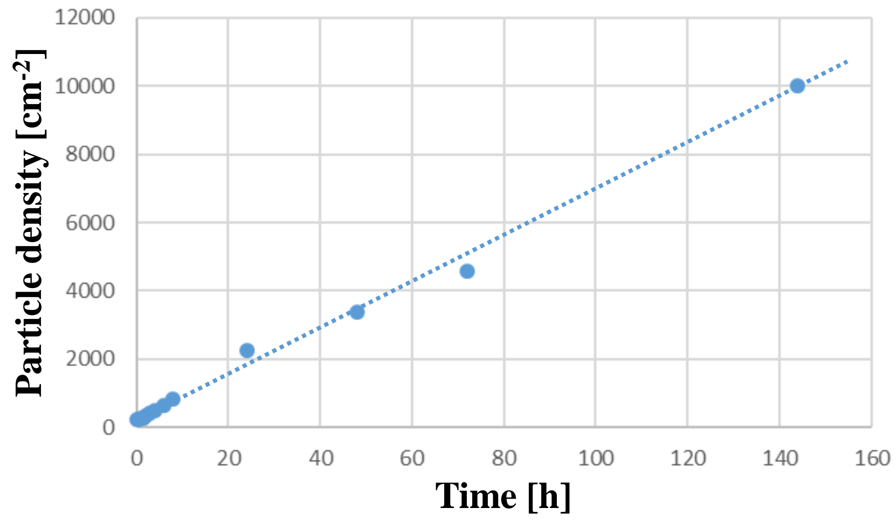

Figure 4. Typical time evolution of the areal particle density on the Si wafer surface.

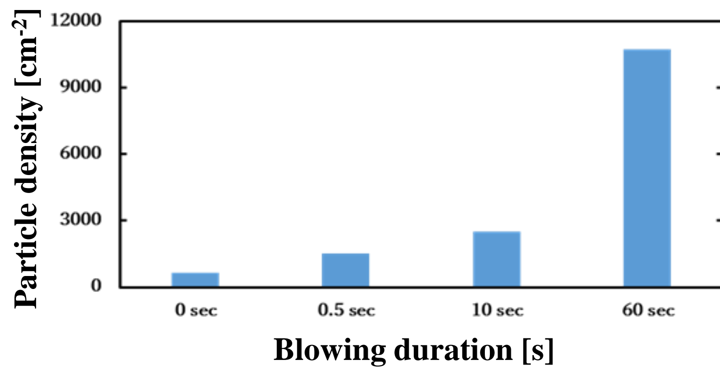

Figure 5. Relationship between the surface particle density and time of blowing onto the wafer surface at the blower air pressure of 0.15 MPa.

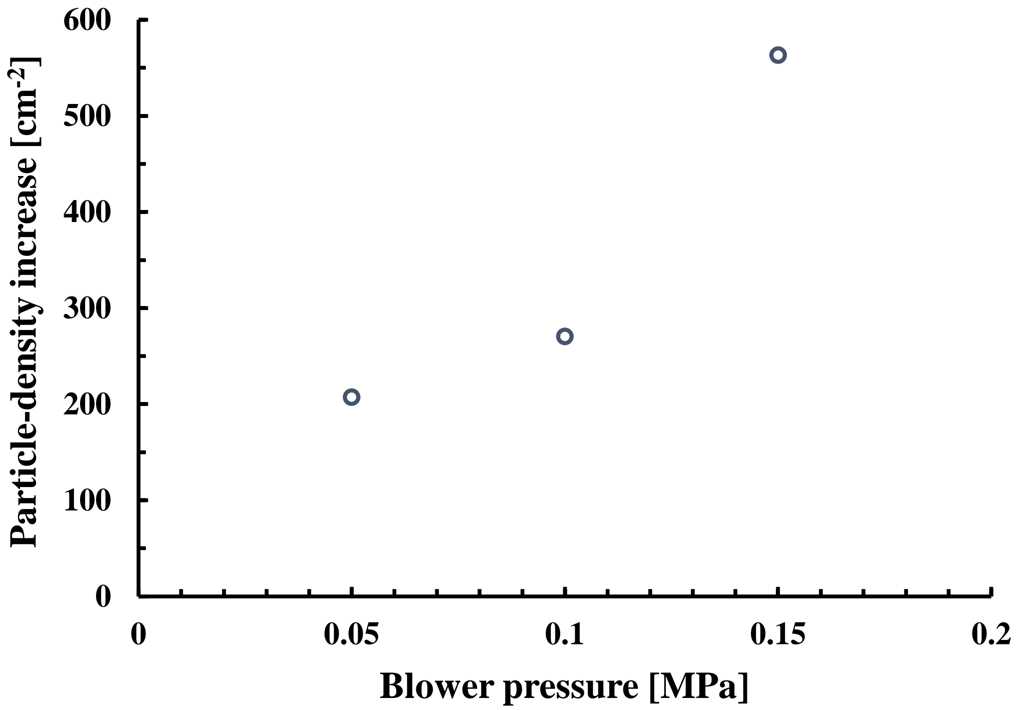

Figure 6. Dependence of the surface-particle-density increase on the air pressure of the blower gun for the blowing times required to complete the removal of water droplets from the Si surfaces.

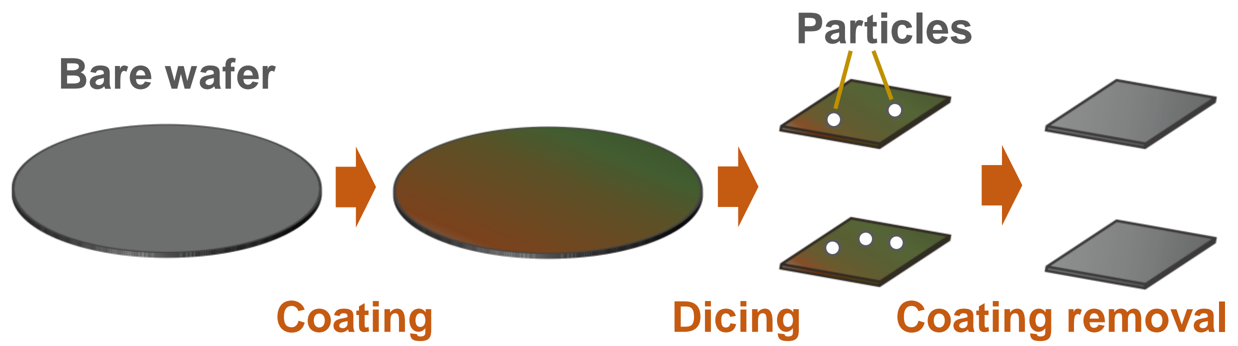

Figure 7. Flow diagram of the surface-coating scheme for the wafer-cutting process.

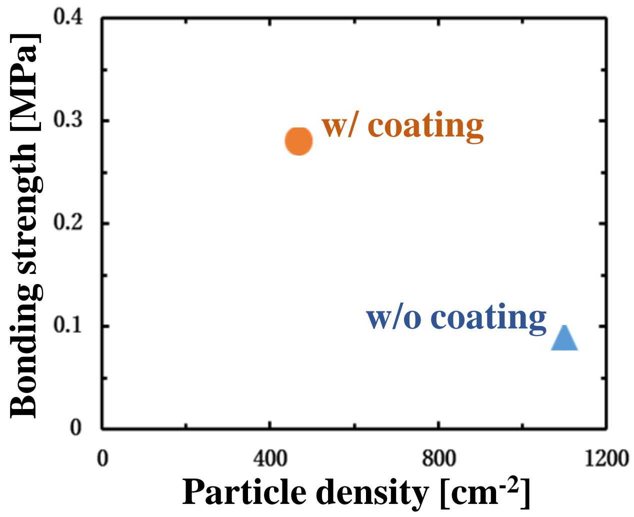

Figure 8. Surface particle densities and bonding strengths for the cases with and without the surface coating treatment in the cutting process.

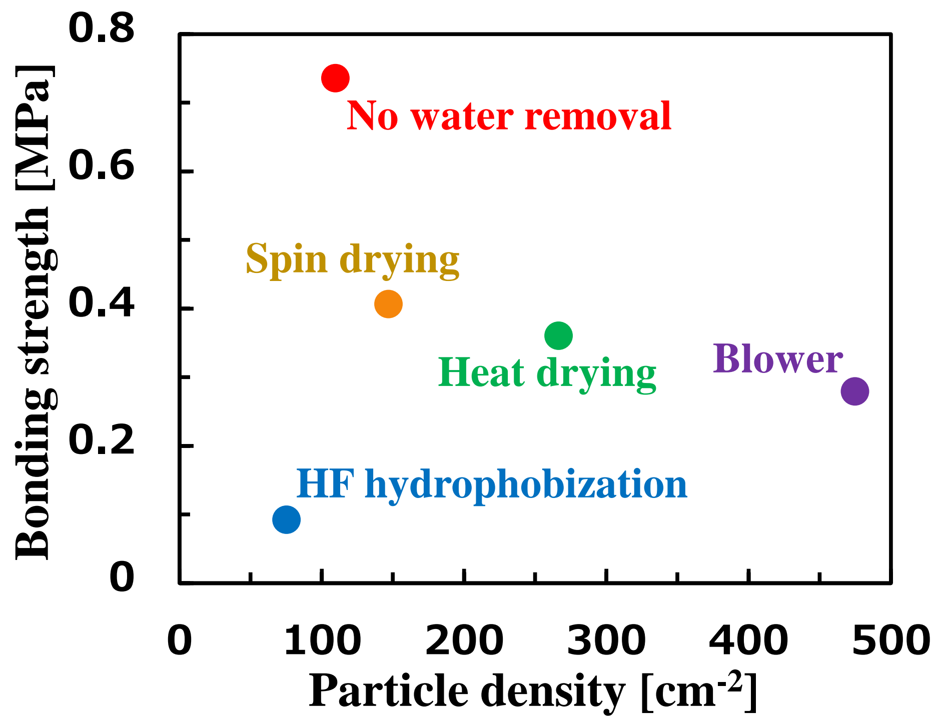

Figure 9. Surface particle density prior to the bonding and mechanical interfacial bonding strength for each drying process condition for the four alternative methods described in the text, along with the case with the conventional blow drying scheme.

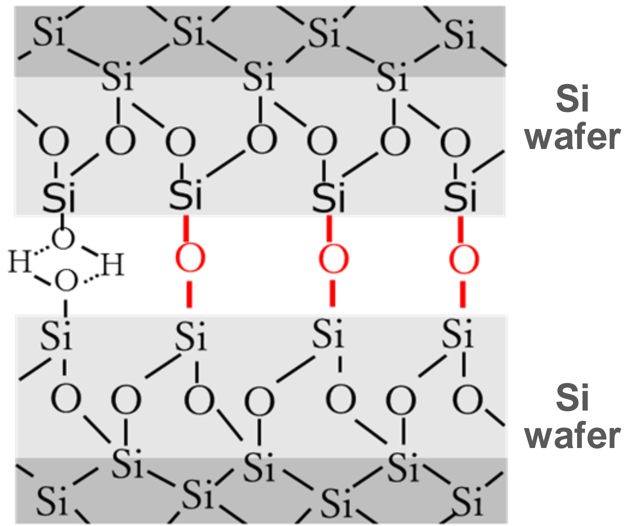

Figure 10. Conceptual schematic of a cross-sectional molecular view of the hydrophilically bonded Si/Si interface.

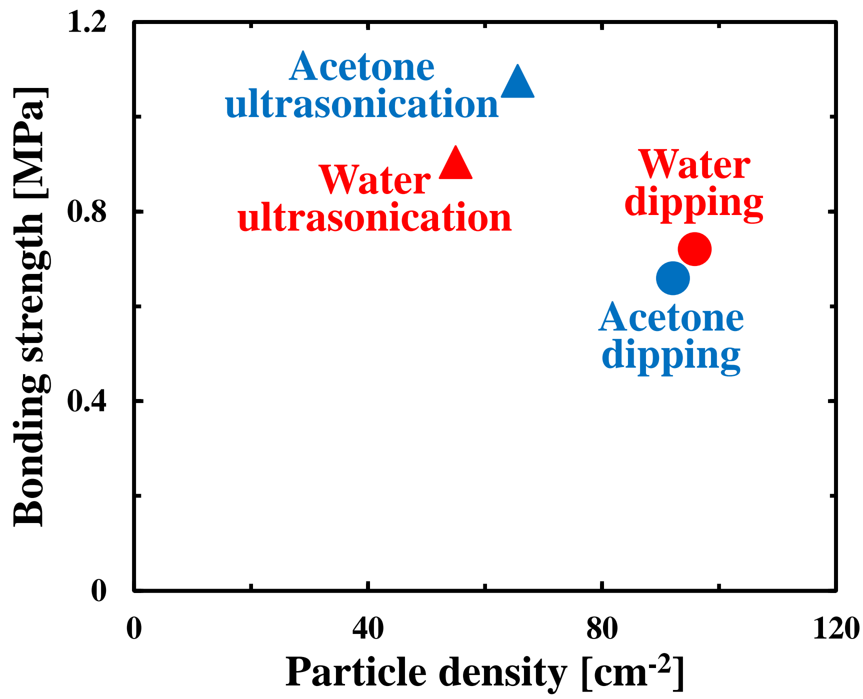

Figure 11. Surface particle density after each surface cleaning treatment with deionized water or acetone with and without sonication for 10 min prior to the bonding and corresponding bonding strength.

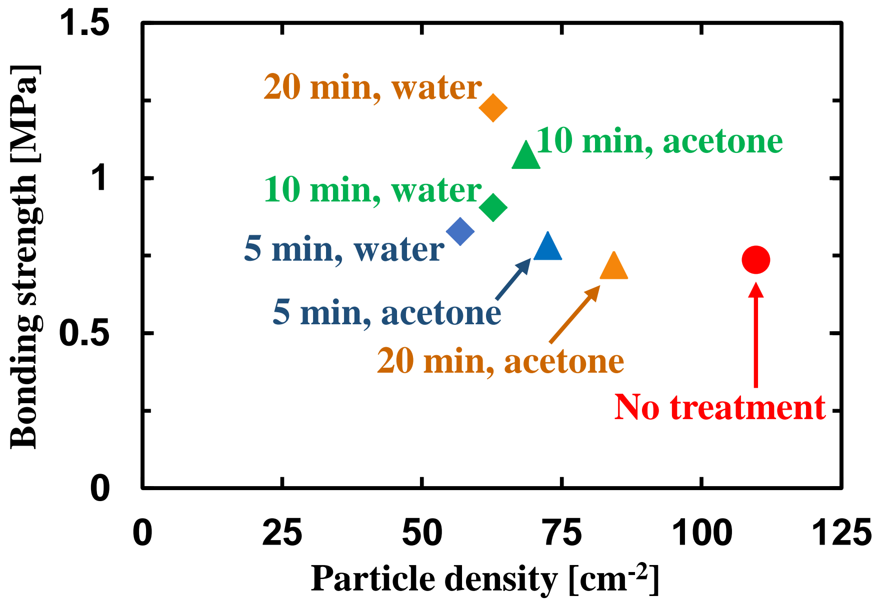

Figure 12. Surface particle density after each sonication prior to the bonding and obtained bonding strength.

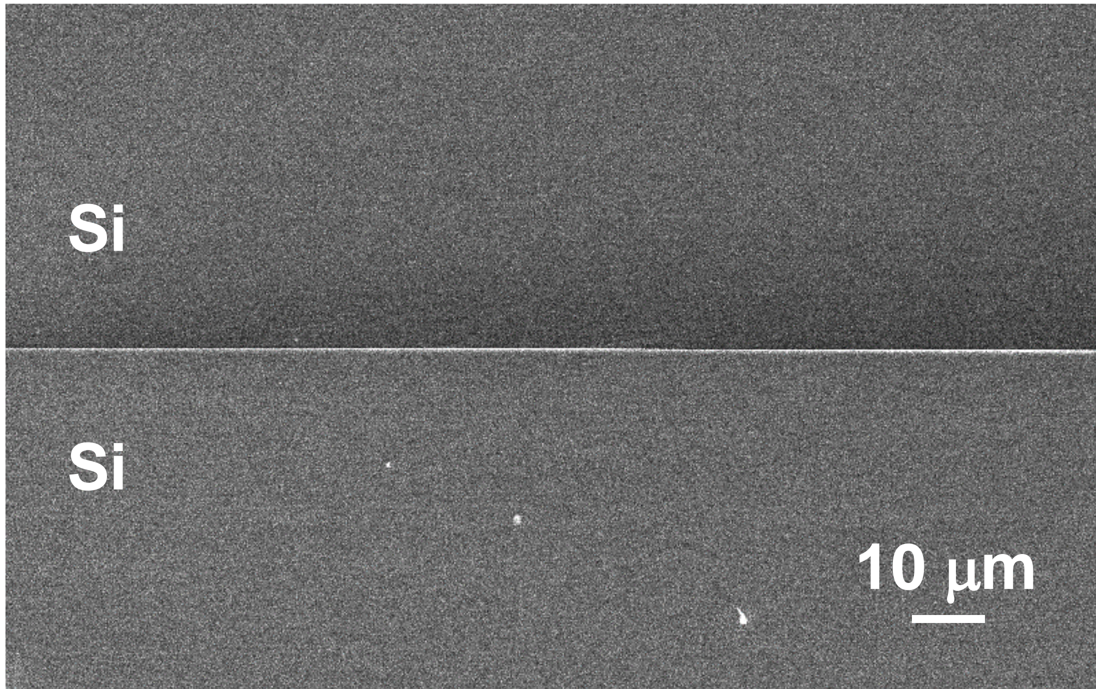

Figure 13. Cross-sectional SEM image of the bonded Si/Si interface.

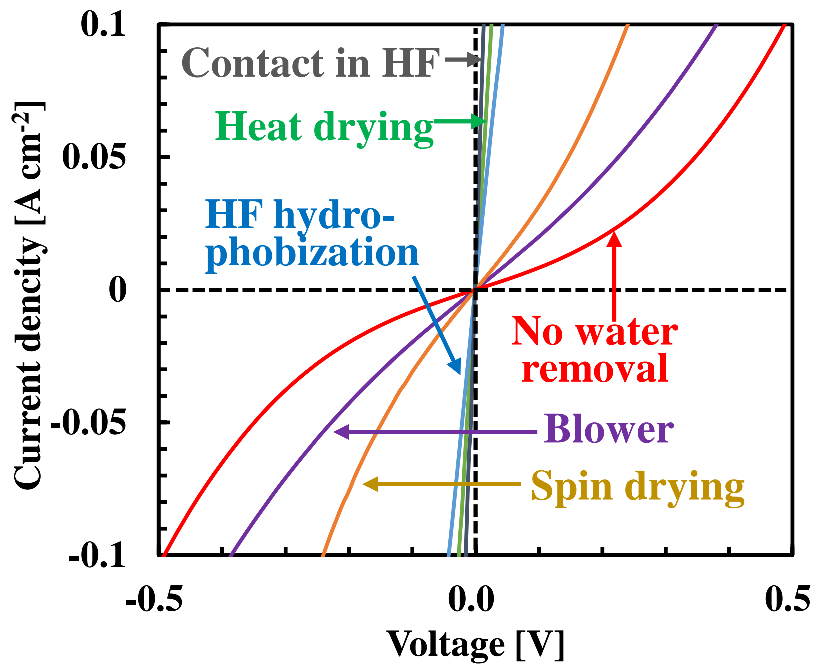

Figure 14. Current–voltage characteristics across the bonded Si/Si interfaces obtained by various surface treatments.

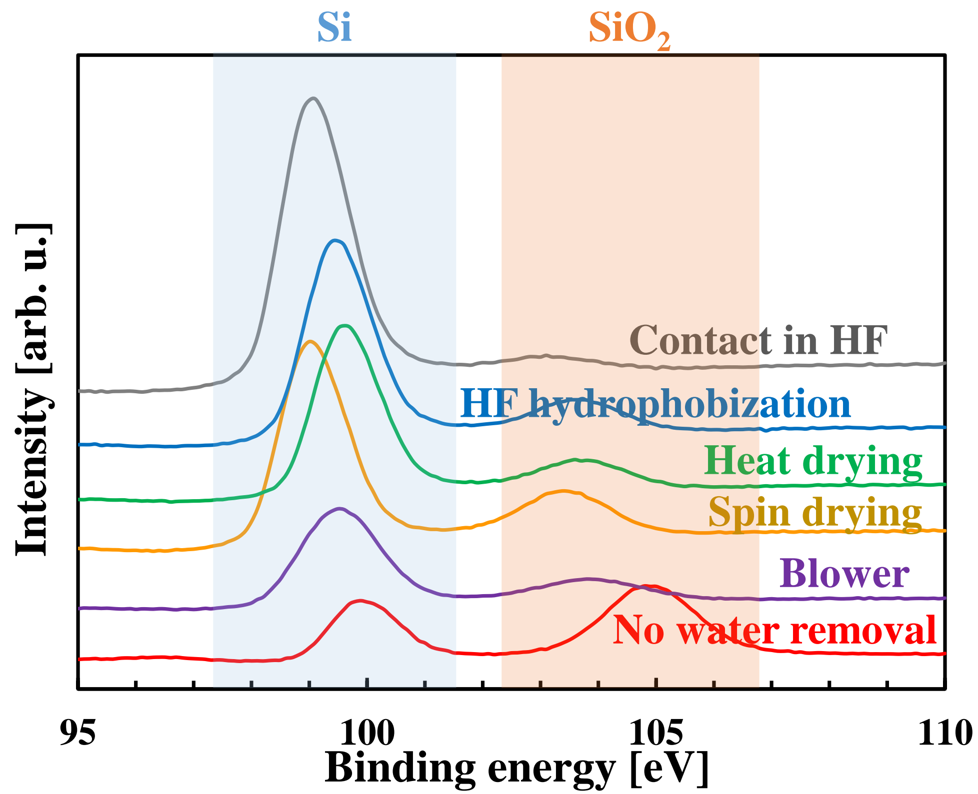

Figure 15. XPS spectra of the debonded Si surfaces immediately after the intentional debonding of the bonded samples obtained by the different pretreatments.

Pretreatment	SiO_2/Si peak area ratio
No water removal	1.72
Blower	0.38
Spin drying	0.37
Heat drying	0.32
HF hydrophobization	0.31
Contact in HF	0.12

Table 1. Ratios of the peak area of SiO_2 to that of Si obtained by XPS measurements (Fig. 15) of the debonded Si surfaces immediately after the intentional debonding of the bonded samples obtained by the different pretreatments.

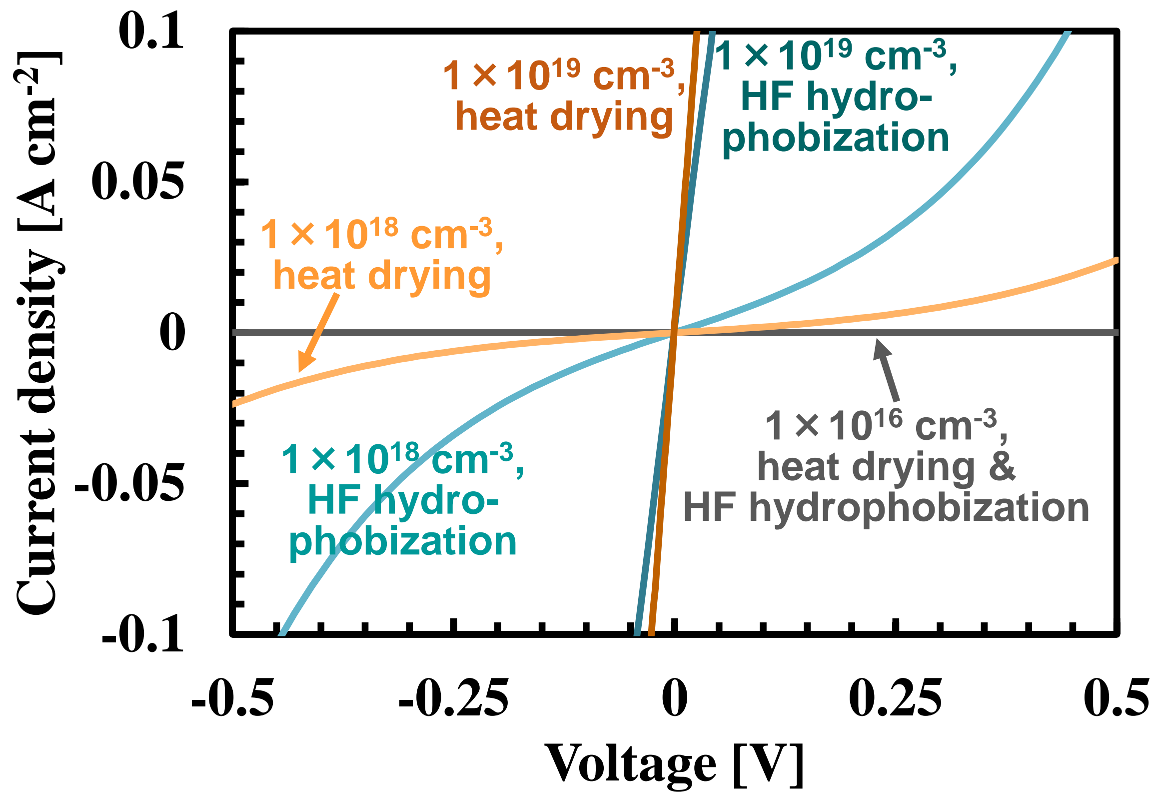

Figure 16. Current–voltage characteristics for the different doping concentrations in the Si wafers for the samples obtained by HF hydrophobization and heat drying.

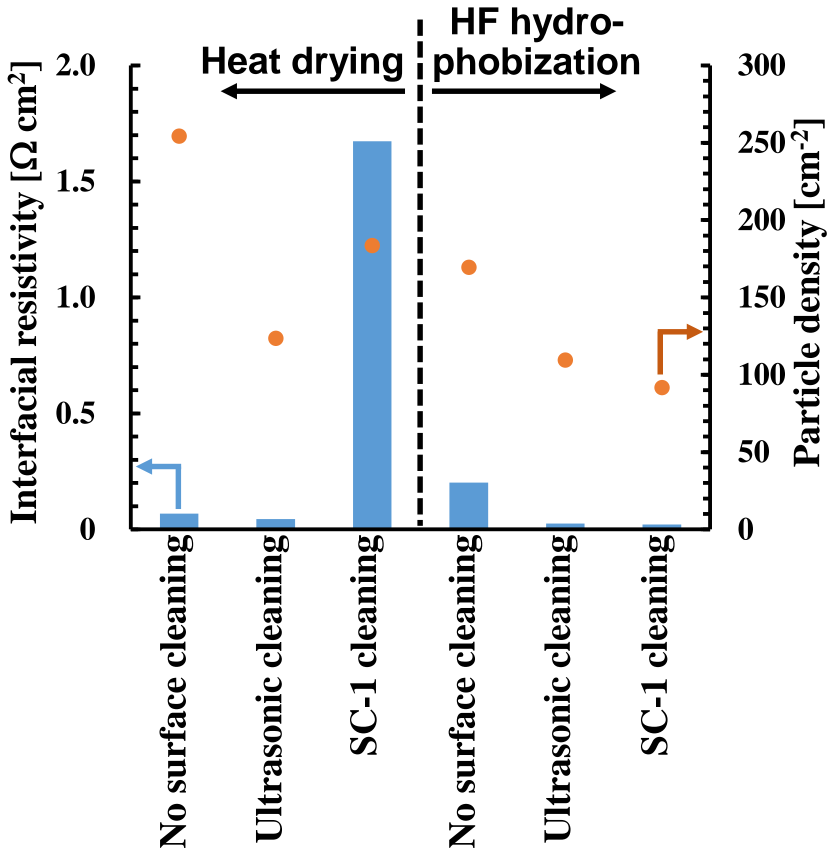

Figure 17. Surface particle densities (dots) and interfacial electrical resistivities (bars) for the cases with the SC-1 cleaning (NH_3:H_2O_2:H_2O = 13:17:70 wt:wt:wt) for 10 min, ultrasonic cleaning in deionized water for 2 min, and without these treatments, for the preparation procedures with the heat drying and HF hydrophobization.

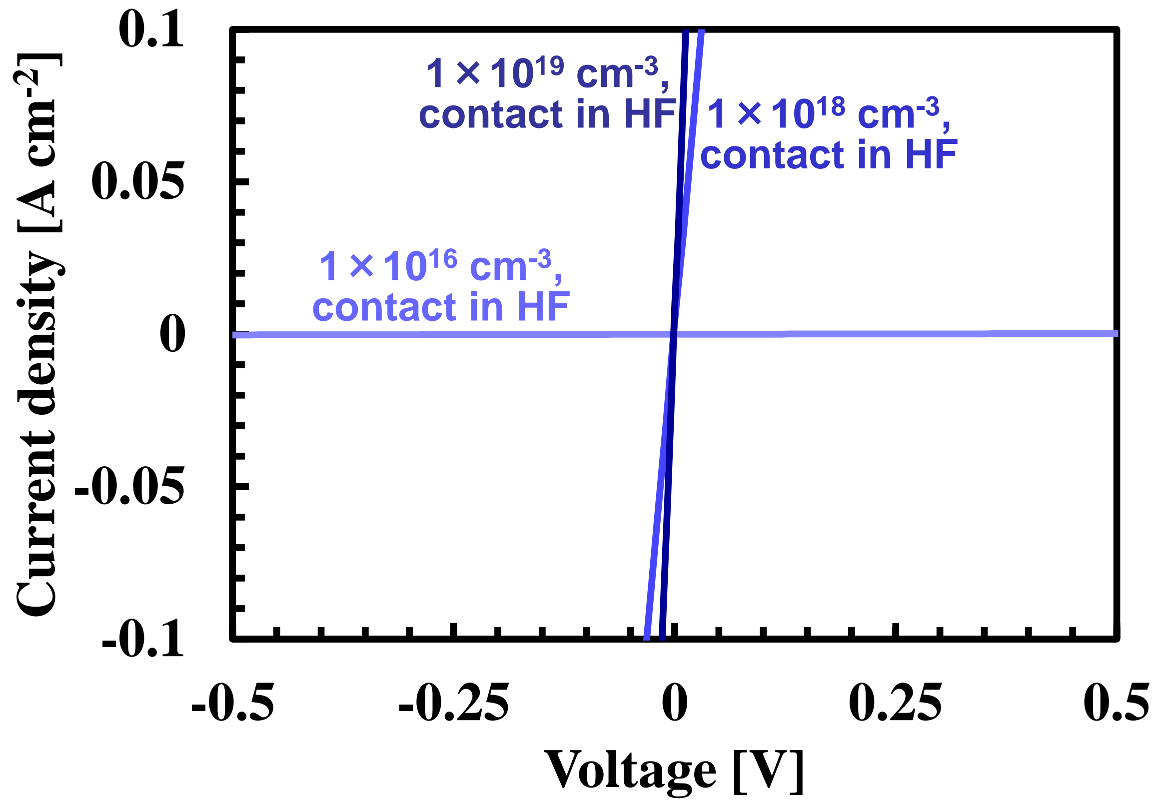

Figure 18. Current–voltage characteristics for the different doping concentrations in the Si wafers for the samples obtained by the procedure including the SC-1 cleaning followed by pre-bonding contacting in HF aq.

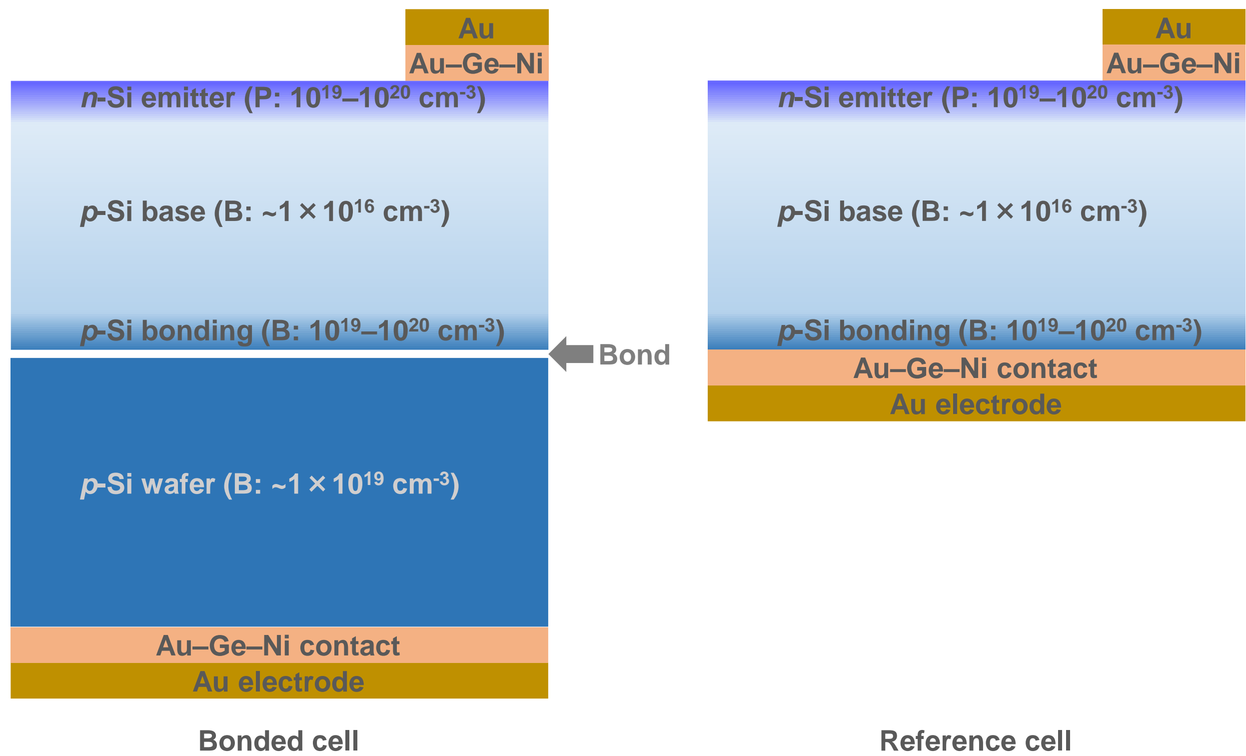

Figure 19. Schematic cross-sectional structural diagrams of the bonded and reference unbonded Si solar cells.

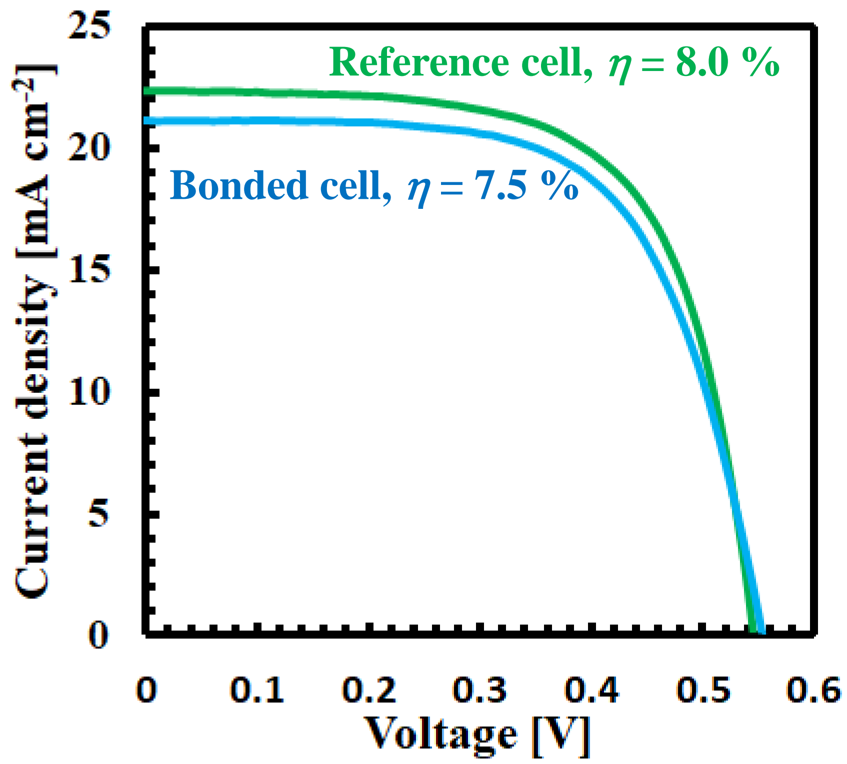

Figure 20. Light current–voltage characteristics of the highest-efficiency bonded and reference unbonded Si solar cells under the AM1.5 G, 1-sun illumination.

	Bonded cell	Reference cell
Average V_{OC}	0.547 V	0.522 V
Average J_{SC}	21.1 mA cm^{-2}	21.2 mA cm^{-2}
Average FF	0.582	0.551
Average η	6.65%	6.18%

Table 2. Average V_{OC}, J_{SC}, FF, and η for the bonded and reference unbonded Si solar cells under the AM1.5 G, 1-sun illumination.

TOC GRAPHIC